THE JOURNAL OF PHYSICAL CHEMISTRY B

Article

pubs.acs.org/JPCB

Thermally Induced Protein Unfolding Probed by Isotope-Edited IR Spectroscopy

Lu Wang and James L. Skinner*

Theoretical Chemistry Institute and Department of Chemistry, University of Wisconsin, Madison, Wisconsin 53706, United States

ABSTRACT: Infrared (IR) spectroscopy has been widely utilized for the study of protein folding, unfolding, and misfolding processes. We have previously developed a theoretical method for calculating IR spectra of proteins in the amide I region. In this work, we apply this method, in combination with replica-exchange molecular dynamics simulations, to study the equilibrium thermal unfolding transition of the villin headpiece subdomain (HP36). Temperature-dependent IR spectra and spectral densities are calculated. The spectral densities correctly reflect the unfolding conformational changes in the simulation. With the help of isotope labeling, we are able to capture the feature that helix 2 of HP36 loses its secondary structure before global unfolding occurs, in agreement with experiment.

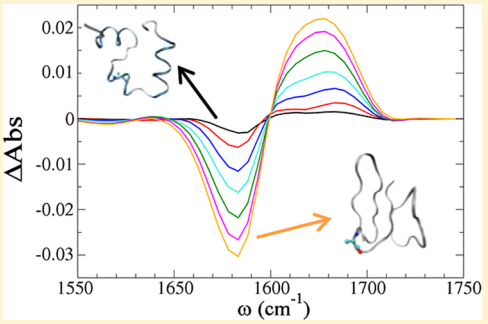

I. INTRODUCTION

The folding of a protein into its unique three-dimensional native structure is essential to its biological function. Many native proteins are only marginally stable, in the sense that small changes in the cellular environment such as temperature and pH may lead to unfolding. Unfolding usually causes a severe reduction in biological activity and can also lead to misfolding, aggregation, and disease.[1−5] Although considerable advances have been made in the study of the structure and dynamics of proteins, unraveling the pathways and mechanisms of protein folding, unfolding, and misfolding processes remains a challenge.[6−18] Such processes involve the rearrangement of a complex network of molecular interactions. Therefore, monitoring these processes *in situ* poses substantial challenges for experiment as it requires techniques that have sufficient structural and time resolution.[12,14,17] Computer simulations complement experiments by providing atomistic details of the structure and dynamics of these processes, although of course they are limited by factors such as force-field accuracy and simulation time scales.[10,13−16]

Infrared (IR) spectroscopy is a highly effective method for probing protein folding, unfolding, and misfolding due to its unique structural and temporal sensitivity.[19−31] IR experiments typically involve the amide I vibrational mode, which is primarily associated with the peptide bond carbonyl stretch[32] and is highly sensitive to protein secondary structure.[19−21] Recent development of time-resolved two-dimensional IR (2DIR) spectroscopy provides subpicosecond time resolution.[22,24−28,33−42] Moreover, residue-specific information can be obtained by using isotope labeling. For example, a $^{13}C{=}^{18}O$ isotope label lowers the amide I frequency by about 70 cm^{-1}.[31,43−55] Carbonyls with $^{13}C{=}^{18}O$ labels are essentially shifted out of the main amide I band and can be resolved individually.

The villin headpiece subdomain, HP36, is a single-domain protein that folds cooperatively. Its small size, simple topology, and fast folding dynamics make it a favorite for experimental and theoretical studies.[56−82] HP36 is part of the villin protein, which spans residues 42 to 76 in the full-length villin headpiece.[56] It has the sequence MLSDEDFKAVFGMTRS**A**-FANLPLWKQQNLKKEKGLF,[56] with the second residue being L42. An additional Met is added to the N-terminus as in the previous experiments and is designated M41.[56,69,72] The C-terminal of F76 is amidated. The native state of HP36 contains three helical segments that pack to form a hydrophobic core, as shown in Figure 1a.[56] Using IR spectroscopy, Brewer et al. studied the thermal unfolding transition of HP36 by monitoring its spectral changes in the temperature range from 7 to 86 °C, with both equilibrium and temperature-jump IR experiments.[69,72] By isotope labeling A57, which is in helix 2, with $^{13}C{=}^{18}O$ as highlighted in the above sequence (in bold) and in Figure 1a, they were able to identify an unfolding of helix 2 before the melting of the entire protein.[72] Their experiments demonstrate the power of IR spectroscopy, in conjunction with isotope labeling, to probe protein folding and unfolding with residue-specific resolution.

Detailed interpretation of experimental IR spectra is facilitated by theoretical calculations. We have recently developed amide I frequency "maps" that allow the calculation of instantaneous frequencies directly from molecular dynamics (MD) simulations.[83] These maps relate amide I frequencies to the local electric fields on the amide groups and were developed for both protein backbone and Asn and Gln side chains. We have combined the frequency maps with established nearest-neighbor frequency shift (NNFS)[84,85] and coupling schemes[84,86] and utilized a mixed quantum/classical approach to calculate protein IR spectra in the amide I region based on MD trajectories.[83] This method provides a means to bridge

Received: May 11, 2012
Revised: July 17, 2012
Published: August 1, 2012

   dx.doi.org/10.1021/jp304613b | *J. Phys. Chem. B* 2012, 116, 9627−9634

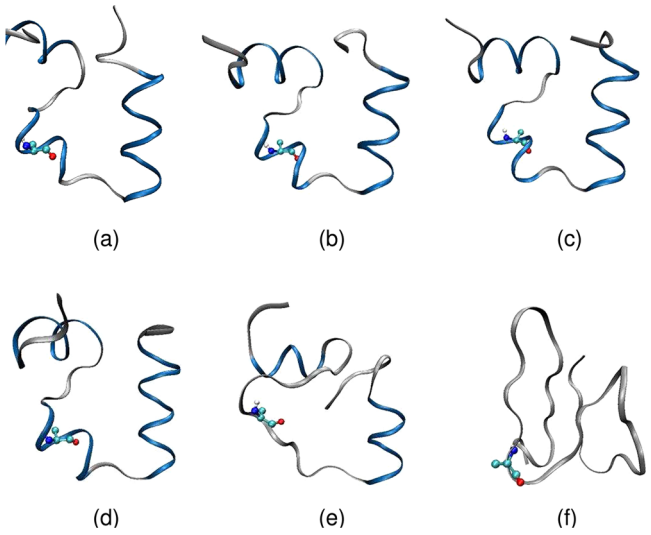

Figure 1. (a) NMR structure of HP36 (Protein Date Bank ID 1VII). Representative structures of HP36 at (b) 7, (c) 45, (d) 77, (e) 116, and (f) 146 °C obtained from cluster analysis of the REMD simulations. α-Helices are shown in blue, and the unstructured parts are shown in gray. A57 is in helix 2 and is highlighted by the stick and ball representation.

spectroscopic experiments and molecular simulations and has the potential to interpret complex experimental spectra at the molecular level. It has been validated by applying to IR spectra of model peptides with various secondary structures[83] and has been shown to reproduce successfully the experimental linear and 2DIR spectra of islet amyloid polypeptide (IAPP),[37,83,87,88] whose misfolding and aggregation are closely related to type 2 diabetes. We have also previously examined[83] the temperature-dependent IR spectra of *N*-methylacetamide, a commonly used model compound to mimic the protein backbone peptide linkage.[89−94] In the present work we focus on HP36 and study its equilibrium thermal unfolding transition using replica-exchange molecular dynamics (REMD) simulations and isotope-edited IR spectral calculations.

The paper is organized as follows. In section II we describe the details of the REMD simulations and the IR calculations. In section III, temperature-dependent IR spectra and spectral densities as well as the thermal unfolding curves of HP36 are presented and compared with experiments. Finally, conclusions are drawn in section IV.

II. THEORETICAL METHODS FOR SPECTRAL CALCULATIONS

REMD simulations have been extensively used in the literature to enhance the conformational sampling of proteins.[95−98] REMD simulations were performed using the GROMACS simulation package.[99−103] 56 replicas were used spanning the temperature range 7−171 °C. The temperatures were chosen to ensure reasonable exchange rates between replicas and were generated using the Web server at http://folding.bmc.uu.se/remd. The initial configuration of HP36 was taken from an NMR structure (Protein Data Bank ID 1VII),[56] as shown in Figure 1a. The structure was modified to include a C-terminal $-NH_2$ cap, consistent with the IR experiments.[69,72] HP36 was put in a cubic box and solvated with 4487 H_2O molecules to ensure a distance of at least 1 nm from all box edges. The protein was modeled using the GROMOS96 53a6 force field,[104−106] and the simple point charge (SPC) model was adopted for water.[107] The protein has a net charge of +3, and chloride ions were added to neutralize it. At each temperature the system was energy minimized, equilibrated in the NVT ensemble for 100 ps and then in the NPT ensemble for 10 ns. REMD simulations with constant temperature and a pressure of 1 bar were performed for 10 ns in each replica. Exchange moves between adjacent replicas were attempted every 2 ps. The Nosé−Hoover thermostat[108,109] and the Parrinello−Rahman barostat[110] were used for the temperature and pressure couplings. The LINCS algorithm was used to constrain all bonds, and the particle-mesh Ewald sum was used to treat long-range electrostatic interactions.[111,112] Configurations from the trajectories of the REMD simulations were saved every 10 fs for spectral calculations.

The theoretical protocol for calculating protein IR spectra in the amide I region has been described elsewhere.[83] Briefly, within the mixed quantum/classical approach, the line shape $I(\omega)$ is given by[113−115]

$$I(\omega) \sim \mathrm{Re} \int_0^\infty \mathrm{d}t\ \mathrm{e}^{-i\omega t} \sum_{ij} \langle m_i(0) F_{ij}(t) m_j(t) \rangle \mathrm{e}^{-t/2T_1} \tag{1}$$

where i and j index the amide I vibrational chromophores. The vibrational Hamiltonian (over $\hbar$) in the amide I region is $\kappa(t)$, whose time propagation is described by the matrix $F(t)$:

$$\dot{F}(t) = iF(t)\kappa(t) \tag{2}$$

with $F_{ij}(0) = \delta_{ij}$. $m_i(t)$ is the projection of the transition dipole moment $\vec{m}_i(t)$ on the polarization unit vector of the excitation light $\hat{\varepsilon}$, i.e., $m_i(t) = \hat{\varepsilon}\cdot\vec{m}_i(t)$. Since in experiment the protein is not oriented, we average over all possible orientations by averaging over the three polarizations $\hat{\varepsilon} = \hat{i},\hat{j},\hat{k}$. The angular brackets in eq 1 indicate a classical equilibrium statistical mechanical average. T_1 is the lifetime of the first excited state of an isolated amide I vibration, and the term $\mathrm{e}^{-t/2T_1}$ is added phenomenologically to incorporate lifetime broadening. T_1 is taken to be 600 fs.[47]

HP36 contains 36 chromophores in the backbone and 4 chromophores in the Asn and Gln side chains. In this case, $\kappa(t)$ is a 40 × 40 matrix, whose diagonal elements are the local frequencies of each chromophore and the off-diagonal elements are the couplings between chromophores. The diagonal elements are obtained by applying the recently developed amide I backbone and side-chain frequency maps,[83] with the 36 backbone chromophores corrected by NNFS.[84,85] Note that since the C-terminal is amidated, the chromophore's frequency for F76 is determined by the side-chain map. The off-diagonal terms are calculated using the nearest-neighbor coupling map[84] or the transition dipole coupling (TDC) method[86] according to the relative positions of the two chromophores.[83] As $\kappa(t)$ is real and symmetric, at any instant in time it can be diagonalized by an orthogonal transformation:

$$P^{\mathrm{T}}\kappa P = \Lambda \tag{3}$$

The diagonal matrix Λ contains the eigenvalues while P is composed of the corresponding eigenvectors. For a specific eigenvalue Λ_{kk}, its corresponding transition dipole is

$$M_k = \sum_i m_i P_{ik} \tag{4}$$

In the inhomogeneous limit where the dynamics is sufficiently slow, we can simply average over an ensemble of static

dx.doi.org/10.1021/jp304613b | J. Phys. Chem. B 2012, 116, 9627−9634

configurations.[113] If we neglect lifetime broadening, eq 1 becomes[113]

$$I(\omega) \sim \sum_k \langle M_k{}^2 \delta(\omega - \Lambda_{kk}) \rangle \tag{5}$$

which is called the spectral density (the frequency distribution weighted by the square of the transition dipole). In a variety of isolated-chromophore systems spectral densities have been demonstrated to capture the essential features of spectra.[113,116−119] We will show that for HP36 the spectral density closely resembles the spectrum, and as it is much simpler to calculate, most analysis in this work is based on the spectral density instead of the spectrum. The A57-labeled IR spectrum and spectral density are calculated by shifting the local frequency of A57 by −70 cm^{-1} [37,43−55,83] and keeping all other parameters the same as in the unlabeled calculations.

III. RESULTS AND DISCUSSION

REMD simulations were run for 10 ns at each of the 56 temperatures, giving a total simulation length of 560 ns. The average exchange probability per attempt is ∼29%. Representative configurations of HP36 are extracted from the REMD simulations using cluster analysis. Figures 1b−f show the configurations most frequently visited at five different temperatures. It is clear that HP36 gradually unfolds as temperature increases. The REMD trajectories were used for spectral calculations at 15 temperatures. Note that at high temperature the unfolded ensemble of HP36 has residual α-helical structure near the N-terminus and is to some extent compact, keeping part of the tertiary contact, in agreement with previous theoretical and experimental results.[67,70,120] These partially folded configurations are sampled in the REMD simulations and are included in the spectral calculations. However, for the purpose of probing the residual secondary and tertiary structures, IR absorption spectroscopy is not ideal as these structures are mostly disordered, and techniques with higher structural sensitivity are required.

Theoretical IR spectra of the unlabeled and A57-labeled HP36 at 7 °C are shown in Figure 2. As expected, incorporating a single label slightly decreases the intensity of the main peak and increases the intensity roughly 70 cm^{-1} to the red. The main peaks in both spectra are at about 1636 cm^{-1}, close to the experimental value of 1645 cm^{-1},[69,72] which is consistent with the primarily α-helical structure of HP36.[23] The A57 isotope peak is at 1570 cm^{-1}, in good agreement with the experimental value of 1572 cm^{-1}.[72] Although the theoretical spectra appear to be less symmetric compared to the experimental amide I bands of HP36 (private communication[72]) and its structural analogue HP35 (which is HP36 without the N-terminal Met),[121] they correctly capture the spectral feature around 1670 cm^{-1}. Spectral analysis reveals that the main peak around 1636 cm^{-1} is due to the unlabeled residues in the three helices, and the shoulder around 1670 cm^{-1} is mainly due to the rest of the unlabeled residues that are unstructured. Residues M53 and L61 are shielded from the surrounding water molecules by the nearby hydrophobic side chains, and as a result they have very high local frequencies and lead to a minor peak around 1700 cm^{-1}.

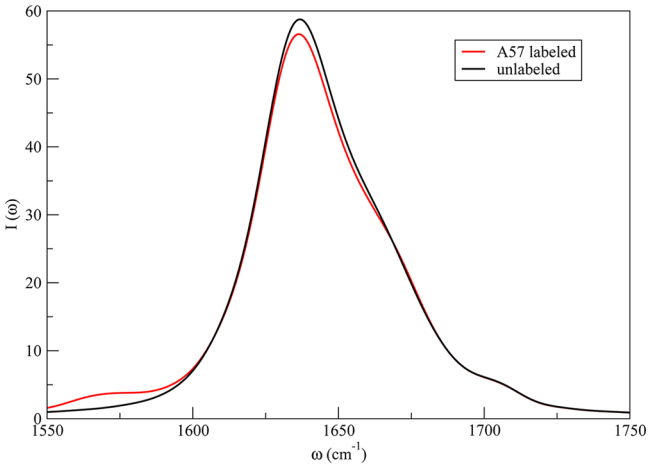

Figure 2. Calculated IR spectra of unlabeled and A57-labeled HP36 at 7 °C.

The spectral density of the A57-labeled HP36 at 7 °C is calculated and compared with the theoretical IR spectrum in Figure 3. The spectral density is a little blue-shifted and broader, but overall it captures the essential features in the spectrum very well and will be used in the following analysis. As the spectral density is the spectrum in the inhomogeneous limit, the good agreement between them indicates that for HP36 at 7 °C the IR spectral features are mainly due to static structural distributions rather than dynamics.

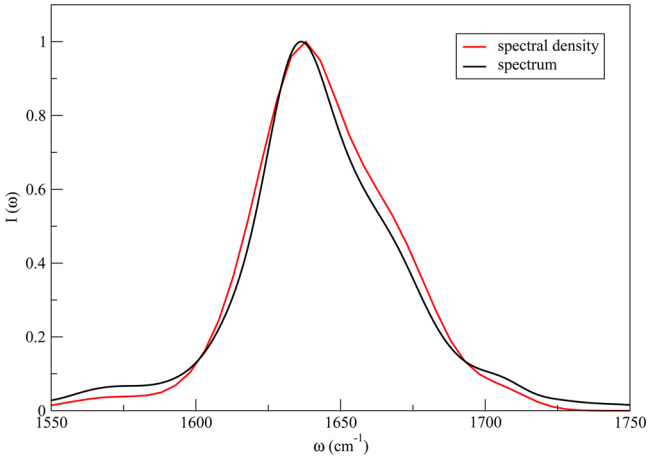

Figure 3. Calculated IR spectrum and spectral density of A57-labeled HP36 at 7 °C. The spectrum and the spectral density are normalized by peak height.

HP36 contains aspartic acid (D) and glutamic acid (E) residues, whose side-chain COO^- asymmetric vibrations absorb near 1600 cm^{-1} and overlap somewhat with the labeled region.[74] We have not included these contributions in our calculations. Note that the D and E peaks do not change much with temperature.[69] In this work we focus on difference spectra, either between unlabeled and A57-labeled HP36 or between different temperatures, in which cases we think the neglect of the D and E contributions is acceptable.

The difference spectrum calculated by subtracting the A57-labeled spectral density from the unlabeled one is shown in Figure 4. The calculation is based on the REMD trajectory at 27 °C, the simulation temperature closest to the experimental condition.[72] As discussed above, isotope labeling A57 leads to an increase in intensity in the isotope region (1550−1600 cm^{-1}) centered at around 1570 cm^{-1}, due to the $^{13}C{=}{=}^{18}O$ stretching mode, and a decrease in intensity in the main peak

dx.doi.org/10.1021/jp304613b | J. Phys. Chem. B 2012, 116, 9627−9634

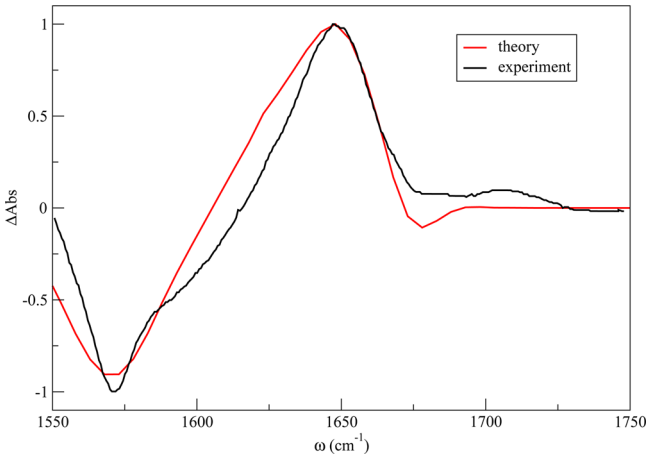

Figure 4. Difference spectrum generated by subtracting the A57-labeled spectrum from the unlabeled spectrum. The theory result is for the spectral density at 27 °C, and experiment is at 25 °C.[72] The theoretical and experimental difference spectra are normalized by their values at the peak near 1650 cm^{-1}.

region (1620−1660 cm^{-1}) centered at 1648 cm^{-1}. Our results agree well with experiment as shown in Figure 4.[72] Note that in experiment the A57-labeled and unlabeled spectra were measured at slightly different pH values, leading to two minor peaks at 1594 and 1704 cm^{-1}.[72] The comparison between theory and experiment verifies that −70 cm^{-1} is a reasonable isotope shift.

Temperature-dependent difference spectra of A57-labeled HP36 are calculated by subtracting the spectral density at 7 °C from the higher temperature ones. Figure 5b shows the results up to 146 °C, which are in qualitative agreement with the experimental data (Figure 5a).[72] From Figures 1b−f we saw that the thermal unfolding process of HP36 involves a conformational change from a folded state containing three α-helices to an unfolded, mainly unstructured state. It is well-known that IR spectra of random coils peak at higher frequencies than those of α-helices.[50] Moreover, it has been shown that increasing temperature leads to the weakening of hydrogen bonds, which consequently leads to a peak shift to higher frequencies in the amide I region.[122] One would therefore expect a blue shift in the spectra as thermal unfolding occurs. Indeed, two pairs of changes are most prominent in Figure 5b. The first pair occurs in the main peak region: a negative feature in the area from 1600−1650 cm^{-1} and a positive feature in the area from 1650−1700 cm^{-1}. These are the spectral manifestations of the loss of secondary and tertiary structure and the increase of disordered regions of the whole protein, respectively. Similarly, the other pair appears in the isotope region: a negative feature from 1550−1580 cm^{-1} and a positive feature from 1580−1600 cm^{-1}. The isotope region probes the A57 behavior and indicates that the part of HP36 that involves A57 loses secondary and tertiary structure and is more disordered in the unfolding process. All features become more prominent with increasing temperatures. In Figure 5a multiple overlapping bands appear in the 1600−1700 regions, probably arising from chromophores in different solvation conditions.[69,72] These features are not visible in Figure 5b, partly due to the fact that spectral densities tend to show averaged features compared to IR spectra. In the IR spectra, which include the motional narrowing effect, we observe a hint of multiple peaks (data not shown), but our theoretical

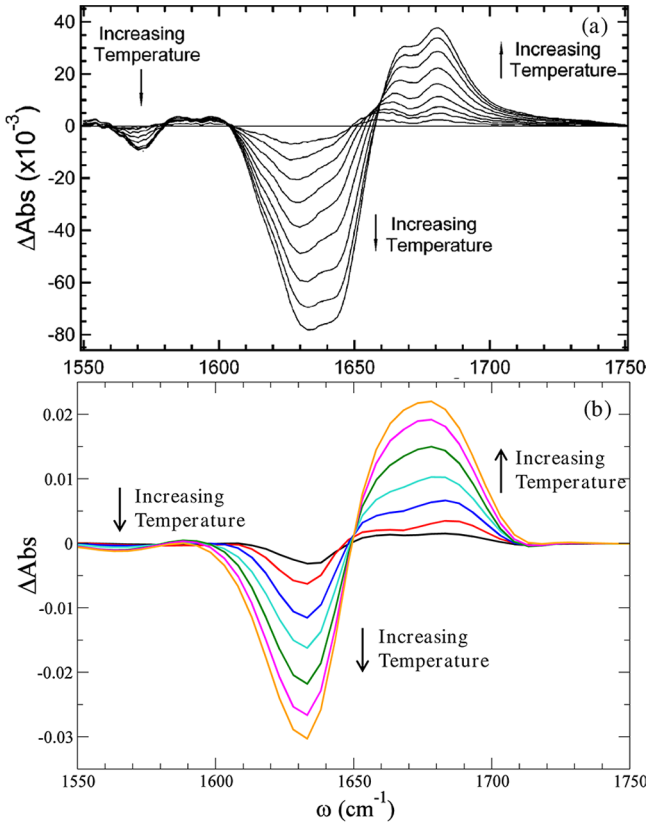

Figure 5. Temperature-dependent difference spectra of A57-labeled HP36. Difference spectrum are calculated by subtracting the spectrum at 7 °C from the higher-temperature spectra. (a) Experimental spectra from 7 to 86 °C in ∼10 °C increments (reprinted with permission from ref 72). (b) Theoretical data for the spectral density from 7 to 146 °C in ∼20 °C increment. The absolute intensities in experiment and theory are in arbitrary units and therefore are not directly comparable.

modeling cannot fully reproduce the experimental features. We will leave this problem to future studies.

In Figure 5b, the negative peaks in the labeled and main regions have frequencies close to 1563 and 1638 cm^{-1}, respectively. The former frequency represents the local behavior of A57, and the latter reflects the whole protein. Choosing these two frequencies, we monitor the intensities ΔAbs as a function of temperature to obtain their melting profiles. Since only one of the 40 chromophores is labeled, the intensity of the isotope peak is about 1/40 that of the main peak. We have normalized ΔAbs at frequencies 1563 and 1638 cm^{-1}, respectively, by their absolute intensities at 7 °C to put them on the same scale for better comparison. The normalized intensity is denoted as $\Delta\mathrm{Abs}_n$. As depicted in Figure 6b, $\Delta\mathrm{Abs}_n$ decreases sigmoidally with temperature. We fit the temperature-dependent $\Delta\mathrm{Abs}_n$ data to a sigmoidal function subjected to the constraint that $\lim_{T\to 7^\circ\mathrm{C}}\Delta\mathrm{Abs}_n = 0$:

$$\Delta\mathrm{Abs}_n = a_1\left[1 - \frac{1 + a_2}{1 + a_2 e^{-a_3(T-7)}}\right] \quad (6)$$

where T is in degrees Celsius and a_1, a_2, and a_3 are fitting parameters. $\Delta\mathrm{Abs}_n$ has the asymptote $\Delta\mathrm{Abs}_{n\infty} \equiv \lim_{T\to\infty}\Delta\mathrm{Abs}_n = -a_1a_2$. The fitted curves are also shown in Figure 6b. The unfolding curve at frequency 1563 cm^{-1} tends to level off at high temperature, while the curve for frequency 1638 cm^{-1}

dx.doi.org/10.1021/jp304613b | J. Phys. Chem. B 2012, 116, 9627−9634

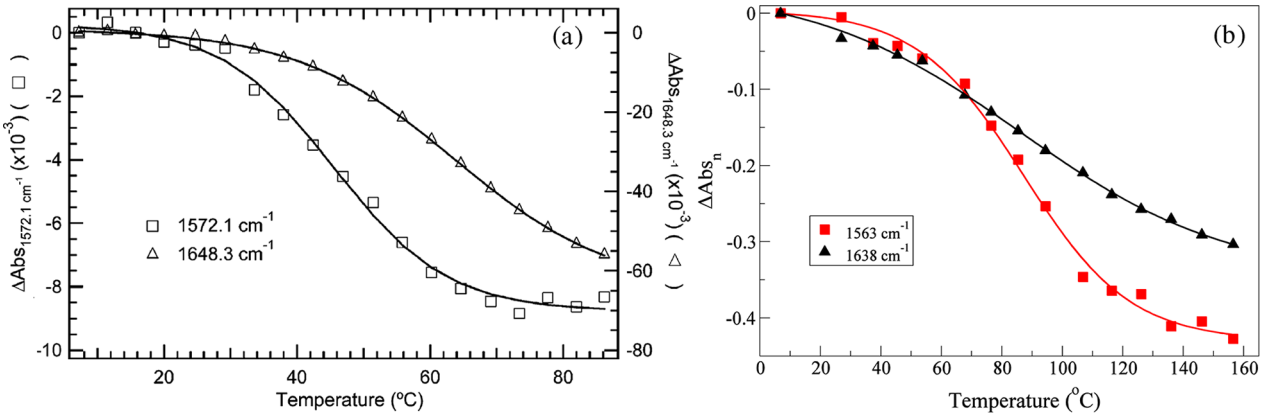

Figure 6. Thermal unfolding transition of A57-labeled HP36 (a) experimentally (reprinted with permission from ref 72) and (b) theoretically. The theoretical results are normalized by the absolute peak intensities at 1563 and 1638 cm^{-1} at 7 °C, respectively. Solid lines are the sigmoidal fit curves.

keeps decreasing in the whole temperature range we study. To quantify the unfolding transition, we have calculated the midpoint of the thermal unfolding transition T_m, which is defined as the temperature at which ΔAbs_n reaches $0.5\Delta Abs_{n\infty}$. T_m for the two frequencies 1563 and 1638 cm^{-1} are 87 and 93 °C, respectively. Experimentally, frequencies of 1572 and 1648 cm^{-1} were used to represent the local and global unfolding transitions of HP36 (Figure 6a).[72] The experimental T_m for frequencies 1572 and 1648 cm^{-1} are about 46 and 64 °C, respectively.[72] Although our melting temperatures are higher than those in experiment, the theoretical unfolding curves are qualitatively in agreement with experiment. We attribute the discrepancies in melting temperature to the inaccuracy of the force field that we are using. The spectra calculations rely on the configurations generated from MD simulations, which are closely related to the force field that defines molecular interactions. As force fields are usually developed for simulations at room temperature, they might predict a different protein unfolding temperature compared to experiment. For example, for the unfolding of the entire HP36 protein, the IR experiment shows a T_m of 64 °C, while the GROMOS96 53a6 (used in this work) and the ECEPP/2 force fields predict values of 93 and 227 °C,[123] respectively. A previous study on HP35 used the AMBER FF03 force field and obtained a T_m of 66 °C, in better agreement with experiment.[124]

The T_m values in theory and experiment imply that helix 2, in which A57 resides, loses its helical structure before the global unfolding occurs. For the purpose of quantifying the unfolding of the three helices, we calculate the temperature-dependent ΔAbs_n for every backbone chromophore, assuming that it is $^{13}C{=}{=}^{18}O$-labeled. Helices 1, 2, and 3 are composed of residues 44−48, 55−58, and 62−71, respectively. Residues that belong to the same helix have similar unfolding behavior, and thus for each helix we average over ΔAbs_n for all its residues, and fit the resulting data to the sigmoidal function in eq 6. We define the percentage decay as $\Delta Abs_n/\Delta Abs_{n\infty}$ and plot it as a function of temperature for the three helices in Figure 7. T_m for helices 1, 2, and 3 are 99, 86, and 92 °C, respectively. From the percentage decay analysis, the thermal unfolding of helix 2 occurs prior to the other two helices. The similarity in T_m's indicates that the unfolding of helix 2 is well represented by A57 and that the decrease of the main peak reflects the average behavior of the protein.

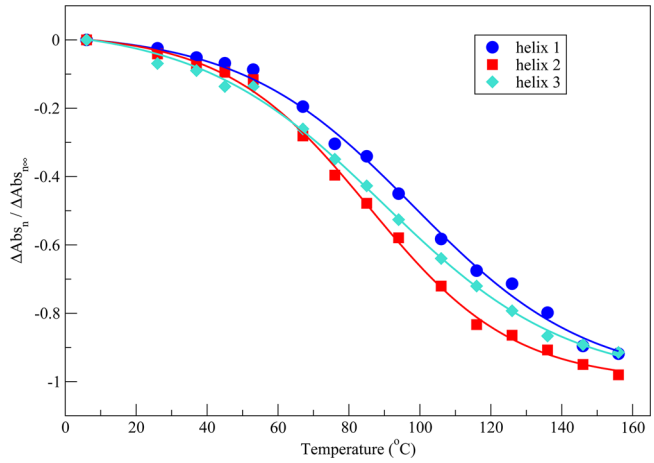

Figure 7. Theoretical thermal unfolding curves for the three helices in HP36. Data for each helix are obtained by averaging over residues belonging to the helix and are normalized to obtain the percentage decay $\Delta Abs_n/\Delta Abs_{n\infty}$ values. Solid lines are the sigmoidal fit curves.

IV. CONCLUSIONS

In this paper, we presented a combined REMD simulation and theoretical IR spectral study of the equilibrium thermal unfolding processes of HP36. The theoretical IR spectra and spectral densities agree quite well with experiments, providing further support for our calculation protocol.[83] With the help of isotope labeling, the thermal unfolding transition of HP36 is followed globally and locally by the decrease of ΔAbs for the main peak and the A57 isotope peak. Theoretical spectral analysis demonstrates that helix 2 loses its secondary structure prior to the global unfolding transition, in agreement with experiment.[72] Although the simulation melting temperatures are not in quantitative agreement with those from experiment,[72] and the difference in the melting temperatures deduced from the labeled and unlabeled peaks in theory (6 °C) is smaller than in experiment (18 °C), the theoretical spectra do correctly reflect the unfolding conformational changes in the simulation. That is to say, when the helices unfold, the spectra shift correspondingly. Discrepancies between theory and experiment are most likely primarily due to inaccuracies of the force field, which is designed to work best close to room temperature (and was applied here at somewhat elevated temperatures), although we cannot rule out contributions from deficiencies in our spectroscopic maps.[83]

dx.doi.org/10.1021/jp304613b | J. Phys. Chem. B 2012, 116, 9627−9634

This work provides one example of utilizing the theoretical strategy we have developed for protein IR calculations for the study of protein unfolding processes. Linear and 2DIR spectroscopy experiments, in combination with the isotope-labeling technique, have the potential to probe protein folding, unfolding, and misfolding processes *in situ* with residue-specific resolution. In a complementary vein, computer simulations, with their increasing power, will help elucidate the structural and dynamical details of such processes. Ours and other theoretical frameworks[36,94,125−127] that allow for the calculation of isotope-edited IR spectra from MD trajectories bridge simulations and experiments and will aid in unraveling the pathways and mechanisms of protein folding, unfolding, and misfolding.

AUTHOR INFORMATION

Corresponding Author

*E-mail: skinner@chem.wisc.edu.

Notes

The authors declare no competing financial interest.

ACKNOWLEDGMENTS

The authors are grateful to Dr. Scott H. Brewer for kindly providing the experimental data. This work was supported in part by a grant from the NSF (CHE-0832584) to J.L.S. J.L.S. also thanks NSF for support of this work through grant CHE-1058752, and NIH, through 1R01DK088184-01A1. This research was also supported in part by the National Science Foundation through XSEDE resources provided by the XSEDE Science Gateways program.

REFERENCES

(1) Nelson, D. L.; Cox, M. M. *Lehninger Principles of Biochemistry*; W.H. Freeman and Company: New York, 2005.
(2) Dobson, C. M. *Trends. Biochem. Sci.* **1999**, *24*, 329−332.
(3) Dobson, C. M. *Nature* **2003**, *426*, 884−890.
(4) Chiti, F.; Dobson, C. M. *Annu. Rev. Biochem.* **2006**, *75*, 333−366.
(5) Thirumalai, D.; Reddy, G.; Straub, J. E. *Acc. Chem. Res.* **2012**, *45*, 83−92.
(6) Dill, K. A. *Biochemistry* **1990**, *29*, 7133−7155.
(7) Straub, J. E.; Thirumalai, D. *Proc. Natl. Acad. Sci. U. S. A.* **1993**, *90*, 809−813.
(8) Šali, A.; Shakhnovich, E.; Karplus, M. *Nature* **1994**, *369*, 248−251.
(9) Onuchic, J. N.; Luthey-Schulten, Z.; Wolynes, P. G. *Annu. Rev. Phys. Chem.* **1997**, *48*, 545−600.
(10) Hummer, G.; Garde, S.; García, A. E.; Paulaitis, M. E.; Pratt, L. R. *J. Phys. Chem. B* **1998**, *102*, 10469−10482.
(11) Shea, J.-E.; Brooks, C. L. *Annu. Rev. Phys. Chem.* **2001**, *52*, 499−535.
(12) Dyson, H. J.; Wright, P. E. *Chem. Rev.* **2004**, *104*, 3607−3622.
(13) Freddolino, P. L.; Harrison, C. B.; Liu, Y.; Schulten, K. *Nat. Phys.* **2010**, *6*, 751−758.
(14) Buchner, G. S.; Murphy, R. D.; Buchete, N.-V.; Kubelka, J. *Biochim. Biophys. Acta* **2011**, *1814*, 1001−1020.
(15) Bowman, G. R.; Voelz, V. A.; Pande, V. S. *Curr. Opin. Struct. Biol.* **2011**, *21*, 4−11.
(16) England, J. L.; Haran, G. *Annu. Rev. Phys. Chem.* **2011**, *62*, 257−277.
(17) Serrano, A. L.; Waegele, M. M.; Gai, F. *Protein Sci.* **2012**, *21*, 157−170.
(18) Culik, R. M.; Jo, H.; DeGrado, W. F.; Gai, F. *J. Am. Chem. Soc.* **2012**, *134*, 8026−8029.
(19) Susi, H.; Byler, D. M. *Methods Enzymol.* **1986**, *130*, 290−311.
(20) Haris, P. I.; Chapman, D. *Trends. Biochem. Sci.* **1992**, *17*, 328−333.
(21) Surewicz, W. K.; Mantsch, H. H.; Chapman, D. *Biochemistry* **1993**, *32*, 389−394.
(22) Zanni, M. T.; Hochstrasser, R. M. *Curr. Opin. Struct. Biol.* **2001**, *11*, 516−522.
(23) Barth, A.; Zscherp, C. *Q. Rev. Biophys.* **2002**, *35*, 369−430.
(24) Hochstrasser, R. M. *Proc. Natl. Acad. Sci. U. S. A.* **2007**, *104*, 14190−14196.
(25) Park, S.; Kwak, K.; Fayer, M. D. *Laser Phys. Lett.* **2007**, *4*, 704−718.
(26) Cho, M. *Chem. Rev.* **2008**, *108*, 1331−1418.
(27) Ganim, Z.; Chung, H. S.; Smith, A. W.; DeFlores, L. P.; Jones, K. C.; Tokmakoff, A. *Acc. Chem. Res.* **2008**, *41*, 432−441.
(28) Strasfeld, D. B.; Ling, Y. L.; Shim, S.-H.; Zanni, M. T. *J. Am. Chem. Soc.* **2008**, *130*, 6698−6699.
(29) Sagle, L. B.; Zimmermann, J.; Dawson, P. E.; Romesberg, F. E. *J. Am. Chem. Soc.* **2006**, *128*, 14232−14233.
(30) Zimmermann, J.; Thielges, M. C.; Yu, W.; Dawson, P. E.; Romesberg, F. E. *J. Phys. Chem. Lett.* **2011**, *2*, 412−416.
(31) Nagarajan, S.; Taskent-Sezgin, H.; Parul, D.; Carrico, I.; Raleigh, D. P.; Dyer, R. B. *J. Am. Chem. Soc.* **2011**, *133*, 20335−20340.
(32) Krimm, S.; Bandekar, J. *Adv. Protein Chem.* **1986**, *38*, 181−364.
(33) Middleton, C. T.; Buchanan, L. E.; Dunkelberger, E. B.; Zanni, M. T. *J. Phys. Chem. Lett.* **2011**, *2*, 2357−2361.
(34) Hamm, P.; Zanni, M. *Concepts and Methods of 2D Infrared Spectroscopy*; Cambridge University Press: Cambridge, UK, 2011.
(35) Jones, K. C.; Ganim, Z.; Peng, C. S.; Tokmakoff, A. *J. Opt. Soc. Am. B* **2012**, *29*, 118−129.
(36) Zhuang, W.; Cui, R. Z.; Silva, D.-A.; Huang, X. *J. Phys. Chem. B* **2011**, *115*, 5415−5424.
(37) Wang, L.; Middleton, C. T.; Singh, S.; Reddy, A. S.; Woys, A. M.; Strasfeld, D. B.; Marek, P.; Raleigh, D. P.; de Pablo, J. J.; Zanni, M. T.; Skinner, J. L. *J. Am. Chem. Soc.* **2011**, *133*, 16062−16071.
(38) Chung, J. K.; Thielges, M. C.; Bowman, S. E. J.; Bren, K. L.; Fayer, M. D. *J. Am. Chem. Soc.* **2011**, *133*, 6681−6691.
(39) Lessing, J.; Roy, S.; Reppert, M.; Baer, M.; Marx, D.; Jansen, T. L. C.; Knoester, J.; Tokmakoff, A. *J. Am. Chem. Soc.* **2012**, *134*, 5032−5035.
(40) Falvo, C.; Zhuang, W.; Kim, Y. S.; Axelsen, P. H.; Hochstrasser, R. M. *J. Phys. Chem. B* **2012**, *116*, 3322−3330.
(41) Moran, S. D.; Woys, A. M.; Buchanan, L. E.; Bixby, E.; Decatur, S. M.; Zanni, M. T. *Proc. Natl. Acad. Sci. U. S. A.* **2012**, *109*, 3329−3334.
(42) Middleton, C. T.; Marek, P.; Cao, P.; Chiu, C.; Singh, S.; Woys, A. M.; de Pablo, J. J.; Raleigh, D. P.; Zanni, M. T. *Nat. Chem.* **2012**, *4*, 355−360.
(43) Torres, J.; Adams, P. D.; Arkin, I. T. *J. Mol. Biol.* **2000**, *300*, 677−685.
(44) Torres, J.; Kukol, A.; Goodman, J. M.; Arkin, I. T. *Biopolymers* **2001**, *59*, 396−401.
(45) Fang, C.; Wang, J.; Charnley, A. K.; Barber-Armstrong, W.; Smith, A. B.; Decatur, S. M.; Hochstrasser, R. M. *Chem. Phys. Lett.* **2003**, *382*, 586−592.
(46) Fang, C.; Wang, J.; Kim, Y. S.; Charnley, A. K.; Barber-Armstrong, W.; Smith, A. B.; Decatur, S. M.; Hochstrasser, R. M. *J. Phys. Chem. B* **2004**, *108*, 10415−10427.
(47) Mukherjee, P.; Krummel, A. T.; Fulmer, E. C.; Kass, I.; Arkin, I. T.; Zanni, M. T. *J. Chem. Phys.* **2004**, *120*, 10215−10224.
(48) Fang, C.; Hochstrasser, R. M. *J. Phys. Chem. B* **2005**, *109*, 18652−18663.
(49) Arkin, I. T. *Curr. Opin. Chem. Biol.* **2006**, *10*, 394−401.
(50) Decatur, S. M. *Acc. Chem. Res.* **2006**, *39*, 169−175.
(51) Mukherjee, P.; Kass, I.; Arkin, I.; Zanni, M. T. *Proc. Natl. Acad. Sci. U. S. A.* **2006**, *103*, 3528−3533.
(52) Mukherjee, P.; Kass, I.; Arkin, I. T.; Zanni, M. T. *J. Phys. Chem. B* **2006**, *110*, 24740−24749.
(53) Shim, S.-H.; Gupta, R.; Ling, Y. L.; Strasfeld, D. B.; Raleigh, D. P.; Zanni, M. T. *Proc. Natl. Acad. Sci. U. S. A.* **2009**, *106*, 6614−6619.

(54) Manor, J.; Mukherjee, P.; Lin, Y.-S.; Leonov, H.; Skinner, J. L.; Zanni, M. T.; Arkin, I. T. *Structure* **2009**, *17*, 247−254.
(55) Woys, A. M.; Lin, Y.-S.; Reddy, A. S.; Xiong, W.; de Pablo, J. J.; Skinner, J. L.; Zanni, M. T. *J. Am. Chem. Soc.* **2010**, *132*, 2832−2838.
(56) McKnight, C. J.; Matsudaira, P. T.; Kim, P. S. *Nat. Struct. Biol.* **1997**, *4*, 180−184.
(57) Duan, Y.; Wang, L.; Kollman, P. A. *Proc. Natl. Acad. Sci. U. S. A.* **1998**, *95*, 9897−9902.
(58) Duan, Y.; Kollman, P. A. *Science* **1998**, *282*, 740−744.
(59) Vugmeyster, L.; Trott, O.; McKnight, C. J.; Raleigh, D. P.; Palmer, A. G. *J. Mol. Biol.* **2002**, *320*, 841−854.
(60) Zagrovic, B.; Snow, C. D.; Khaliq, S.; Shirts, M. R.; Pande, V. S. *J. Mol. Biol.* **2002**, *323*, 153−164.
(61) van der Spoel, D.; Lindahl, E. *J. Phys. Chem. B* **2003**, *107*, 11178−11187.
(62) Lin, C.-Y.; Hu, C.-K.; Hansmann, U. H. E. *Proteins* **2003**, *52*, 436−445.
(63) Wang, M.; Tang, Y.; Sato, S.; Vugmeyster, L.; McKnight, C. J.; Raleigh, D. P. *J. Am. Chem. Soc.* **2003**, *125*, 6032−6033.
(64) Kubelka, J.; Eaton, W. A.; Hofrichter, J. *J. Mol. Biol.* **2003**, *329*, 625−630.
(65) Jang, S.; Kim, E.; Shin, S.; Pak, Y. *J. Am. Chem. Soc.* **2003**, *125*, 14841−14846.
(66) Ripoll, D. R.; Vila, J. A.; Scheraga, H. A. *J. Mol. Biol.* **2004**, *339*, 915−925.
(67) Tang, Y.; Rigotti, D. J.; Fairman, R.; Raleigh, D. P. *Biochemistry* **2004**, *43*, 3264−3272.
(68) Chiu, T. K.; Kubelka, J.; Herbst-Irmer, R.; Eaton, W. A.; Hofrichter, J.; Davies, D. R. *Proc. Natl. Acad. Sci. U. S. A.* **2005**, *102*, 7517−7522.
(69) Brewer, S. H.; Vu, D. M.; Tang, Y.; Li, Y.; Franzen, S.; Raleigh, D. P.; Dyer, R. B. *Proc. Natl. Acad. Sci. U. S. A.* **2005**, *102*, 16662−16667.
(70) Tang, Y.; Goger, M. J.; Raleigh, D. P. *Biochemistry* **2006**, *45*, 6940−6946.
(71) Tang, Y.; Grey, M. J.; McKnight, J.; Palmer, A. G.; Raleigh, D. P. *J. Mol. Biol.* **2006**, *355*, 1066−1077.
(72) Brewer, S. H.; Song, B.; Raleigh, D. P.; Dyer, R. B. *Biochemistry* **2007**, *46*, 3279−3285.
(73) Bi, Y.; Cho, J.-H.; Kim, E.-Y.; Shan, B.; Schindelin, H.; Raleigh, D. P. *Biochemistry* **2007**, *46*, 7497−7505.
(74) Bagchi, S.; Falvo, C.; Mukamel, S.; Hochstrasser, R. M. *J. Phys. Chem. B* **2009**, *113*, 11260−11273.
(75) Meng, W.; Shan, B.; Tang, Y.; Raleigh, D. P. *Protein Sci.* **2009**, *18*, 1692−1701.
(76) Xiao, S.; Bi, Y.; Shan, B.; Raleigh, D. P. *Biochemistry* **2009**, *48*, 4607−4616.
(77) Wei, H.; Yang, L.; Gao, Y. Q. *J. Phys. Chem. B* **2010**, *114*, 11820−11826.
(78) Chung, J. K.; Thielges, M. C.; Fayer, M. D. *Proc. Natl. Acad. Sci. U. S. A.* **2011**, *108*, 3578−3583. Chung, J. K.; Thielges, M. C.; Fayer, M. D. *J. Am. Chem. Soc.* **2012**, *134*, 12118−12124.
(79) Beauchamp, K. A.; Ensign, D. L.; Das, R.; Pande, V. S. *Proc. Natl. Acad. Sci. U. S. A.* **2011**, *108*, 12734−12739.
(80) Urbanek, D. C.; Vorobyev, D. Y.; Serrano, A. L.; Gai, F.; Hochstrasser, R. M. *J. Phys. Chem. Lett.* **2010**, *1*, 3311−3315.
(81) Roy, S.; Bagchi, B. *J. Phys. Chem. B* **2012**, *116*, 2958−2968.
(82) Lv, C.; Tan, C.; Qin, M.; Zou, D.; Cao, Y.; Wang, W. *Biophys. J.* **2012**, *102*, 1944−1951.
(83) Wang, L.; Middleton, C. T.; Zanni, M. T.; Skinner, J. L. *J. Phys. Chem. B* **2011**, *115*, 3713−3724.
(84) Jansen, T. L. C.; Dijkstra, A. G.; Watson, T. M.; Hirst, J. D.; Knoester, J. *J. Chem. Phys.* **2006**, *125*, 044312.
(85) Jansen, T. L. C. *J. Chem. Phys.* **2012**, *136*, 209901.
(86) Torii, H.; Tasumi, M. *J. Raman Spectrosc.* **1998**, *29*, 81−86.
(87) Reddy, A. S.; Wang, L.; Lin, Y.-S.; Ling, Y.; Chopra, M.; Zanni, M. T.; Skinner, J. L.; de Pablo, J. J. *Biophys. J.* **2010**, *98*, 443−451.
(88) Reddy, A. S.; Wang, L.; Singh, S.; Ling, Y. L.; Buchanan, L.; Zanni, M. T.; Skinner, J. L.; de Pablo, J. J. *Biophys. J.* **2010**, *99*, 2208−2216.
(89) Ham, S.; Kim, J.-H.; Lee, H.; Cho, M. *J. Chem. Phys.* **2003**, *118*, 3491−3498.
(90) Schmidt, J. R.; Corcelli, S. A.; Skinner, J. L. *J. Chem. Phys.* **2004**, *121*, 8887−8896.
(91) Hayashi, T.; Zhuang, W.; Mukamel, S. *J. Phys. Chem. A* **2005**, *109*, 9747−9759.
(92) Jansen, T. L. C.; Knoester, J. *J. Chem. Phys.* **2006**, *124*, 044502.
(93) Lin, Y.-S.; Shorb, J. M.; Mukherjee, P.; Zanni, M. T.; Skinner, J. L. *J. Phys. Chem. B* **2009**, *113*, 592−602.
(94) Maekawa, H.; Ge, N.-H. *J. Phys. Chem. B* **2010**, *114*, 1434−1446.
(95) Sugita, Y.; Okamoto, Y. *Chem. Phys. Lett.* **1999**, *314*, 141−151.
(96) Sanbonmatsu, K. Y.; García, A. E. *Proteins* **2002**, *46*, 225−234.
(97) Rathore, N.; Chopra, M.; de Pablo, J. J. *J. Chem. Phys.* **2005**, *122*, 024111.
(98) Chebaro, Y.; Dong, X.; Laghaei, R.; Derreumaux, P.; Mousseau, N. *J. Phys. Chem. B* **2009**, *113*, 267−274.
(99) Bekker, H.; Berendsen, H. J. C.; Dijkstra, E. J.; Achterop, S.; van Drunen, R.; van der Spoel, D.; Sijbers, A.; Keegstra, H.; Reitsma, B.; Renardus, M. K. R. In *Physics Computing 92*; Groot, R. A., Nadrchal, J., Eds.; World Scientific: Singapore, 1993.
(100) Berendsen, H. J. C.; van der Spoel, D.; van Drunen, R. *Comput. Phys. Commun.* **1995**, *91*, 43−56.
(101) Lindahl, E.; Hess, B.; van der Spoel, D. *J. Mol. Model.* **2001**, *7*, 306−317.
(102) van der Spoel, D.; Lindahl, E.; Hess, B.; van Buuren, A. R.; Apol, E.; Meulenhoff, P. J.; Tieleman, D. P.; Sijbers, A. L. T. M.; Feenstra, K. A.; van Drunen, R.; Berendsen, H. J. C. *Gromacs User Manual, version 3.3*; www.gromacs.org, 2005.
(103) van der Spoel, D.; Lindahl, E.; Hess, B.; Groenhof, G.; Mark, A. E.; Berendsen, H. J. C. *J. Comput. Chem.* **2005**, *26*, 1701−1718.
(104) van Gunsteren, W. F.; Billeter, S. R.; Eising, A. A.; Hünenberger, P. H.; Krüger, P.; Mark, A. E.; Scott, W. R. P.; Tironi, I. G. *Biomolecular Simulation: The GROMOS96 Manual and User Guide*; Hochschuleverlag AG an der ETH Zürich: Zürich, Switzerland, 1996.
(105) Scott, W. R. P.; Hünenberger, P. H.; Tironi, I. G.; Mark, A. E.; Billeter, S. R.; Fennen, J.; Torda, A. E.; Huber, T.; Krüger, P.; van Gunsteren, W. F. *J. Phys. Chem. A* **1999**, *103*, 3596−3607.
(106) Oostenbrink, C.; Villa, A.; Mark, A. E.; van Gunsteren, W. F. *J. Comput. Chem.* **2004**, *25*, 1656−1676.
(107) Berendsen, H. J. C.; Postma, J. P. M.; van Gunsteren, W. F.; Hermans, J. In *Intermolecular Forces*; Pullman, B., Ed.; Reidel: Dordrecht, 1981.
(108) Nosé, S. *J. Chem. Phys.* **1984**, *81*, 511−519.
(109) Hoover, W. G. *Phys. Rev. A* **1985**, *31*, 1695−1697.
(110) Parrinello, M.; Rahman, A. *J. Appl. Phys.* **1981**, *52*, 7182−7190.
(111) Darden, T.; York, D.; Pedersen, L. *J. Chem. Phys.* **1993**, *98*, 10089−10092.
(112) Essmann, U.; Perera, L.; Berkowitz, M. L.; Darden, T.; Lee, H.; Pedersen, L. G. *J. Chem. Phys.* **1995**, *103*, 8577−8593.
(113) Auer, B. M.; Skinner, J. L. *J. Chem. Phys.* **2007**, *127*, 104105.
(114) Auer, B. M.; Skinner, J. L. *J. Chem. Phys.* **2008**, *128*, 224511.
(115) Mukamel, S. *Principles of Nonlinear Optical Spectroscopy*; Oxford: New York, 1995.
(116) Auer, B. M.; Skinner, J. L. *J. Chem. Phys.* **2008**, *129*, 214705.
(117) Pieniazek, P. A.; Tainter, C. J.; Skinner, J. L. *J. Am. Chem. Soc.* **2011**, *133*, 10360−10363.
(118) Pieniazek, P. A.; Tainter, C. J.; Skinner, J. L. *J. Chem. Phys.* **2011**, *135*, 044701.
(119) Skinner, J. L.; Pieniazek, P. A.; Gruenbaum, S. M. *Acc. Chem. Res.* **2012**, *45*, 93−100.
(120) Wickstrom, L.; Okur, A.; Song, K.; Hornak, V.; Raleigh, D. P.; Simmerling, C. L. *J. Mol. Biol.* **2006**, *360*, 1094−1107.
(121) Bunagan, M. R.; Gao, J.; Kelly, J. W.; Gai, F. *J. Am. Chem. Soc.* **2009**, *131*, 7470−7476.

(122) Mukherjee, S.; Chowdhury, P.; Gai, F. *J. Phys. Chem. B* **2007**, *111*, 4596−4602.
(123) Trebst, S.; Troyer, M.; Hansmann, U. H. E. *J. Chem. Phys.* **2006**, *124*, 174903.
(124) Lei, H.; Wu, C.; Liu, H.; Duan, Y. *Proc. Natl. Acad. Sci. U. S. A.* **2007**, *104*, 4925−4930.
(125) Zhuang, W.; Abramavicius, D.; Hayashi, T.; Mukamel, S. *J. Phys. Chem. B* **2006**, *110*, 3362−3374.
(126) Zhuang, W.; Hayashi, T.; Mukamel, S. *Angew. Chem., Int. Ed.* **2009**, *48*, 3750−3781.
(127) Smith, A. W.; Lessing, J.; Ganim, Z.; Peng, C. S.; Tokmakoff, A.; Roy, S.; Jansen, T. L. C.; Knoester, J. *J. Phys. Chem. B* **2010**, *114*, 10913−10924.